

# Structural characterisation of X-ray amorphous calcium carbonate (ACC) in sternal deposits of the crustacea *Porcellio scaber*

Alexander Becker,<sup>a</sup> Ulrich Bismayer,<sup>b</sup> Matthias Epple,<sup>\*a</sup> Helge Fabritius,<sup>c</sup> Bernd Hasse,<sup>a</sup> Jianmin Shi<sup>b</sup> and Andreas Ziegler<sup>\*c</sup>

<sup>a</sup> Solid State Chemistry, Faculty of Chemistry, University of Bochum, D-44780 Bochum, Germany. E-mail: matthias.epple@ruhr-uni-bochum.de

<sup>b</sup> Institute for Mineralogy and Petrography, University of Hamburg, Grindelallee 48, D-20146 Hamburg, Germany

<sup>c</sup> Central Facility for Electron Microscopy, University of Ulm, Albert-Einstein-Allee 11, D-89069 Ulm, Germany. E-mail: andreas.ziegler@medizin.uni-ulm.de

Received 25th October 2002, Accepted 2nd January 2003

First published as an Advance Article on the web 23rd January 2003

Mineral deposits in land-based woodlice (crustacea, *Porcellio scaber*) were analysed by high-resolution X-ray diffraction, X-ray absorption spectroscopy (EXAFS) and infrared microscopy. Calcium carbonate is stored within the first four anterior sternites before changing the cuticle (shell). These deposits consist of fully X-ray amorphous calcium carbonate (primary particle size less than 100 Å). The short-range order is comparable to crystalline calcium carbonate phases (first coordination shell), but there is increasing structural disorder beyond about 3 Å. This high degree of structural disorder gives a high solubility, *i.e.* an easy mobilisation within the biological system. The results are compared with EXAFS data from the literature on other biogenic amorphous calcium carbonates.

## Introduction

Inorganic minerals are used in many biological systems for different purposes, with teeth, bones and shells being only the most prominent examples.<sup>1–6</sup> While many biominerals occur in a crystalline form (like molluscan shells consisting of CaCO<sub>3</sub> in its calcitic or aragonitic modification) there are a number of cases where the biomineral is X-ray amorphous (like in all structures consisting of silica: SiO<sub>2</sub>·*n*H<sub>2</sub>O). In the last decade the attention has increasingly turned to amorphous phases that earlier remained mostly undetected due to a lack of suitable analytical techniques.

In particular, recent investigations suggest that amorphous CaCO<sub>3</sub> plays an important role in the initiation of the biomineralisation process. Because the solubility of amorphous CaCO<sub>3</sub> is about ten times higher than that of crystalline CaCO<sub>3</sub>,<sup>7</sup> it can be used as temporary storage for calcium. Although amorphous CaCO<sub>3</sub> is unstable *in vitro*, it is quite stable in some biominerals, and an increasing number of reports indicate that amorphous CaCO<sub>3</sub> occurs in a variety of biological systems, be it as precursor phase on the way to crystalline calcium carbonate,<sup>8–12</sup> as final biomineralised product,<sup>13–17</sup> or for intermediate storage of calcium.<sup>18–20</sup> It has been detected *inter alia* in woodlice of the type *Oniscus asellus*,<sup>18</sup> in plant cystoliths in the leaf of *Ficus retusa*<sup>13</sup> and *Ficus microcarpa*,<sup>17</sup> in larval shells of the freshwater snail *Biomphalaria glabrata*<sup>9,11</sup> and of the marine bivalves *Mercenaria mercenaria*<sup>12</sup> and *Crassostrea gigas*,<sup>12</sup> in body spicules of the ascidian *Pyura pachydermatina*,<sup>15,17</sup> and in the carapace of the american lobster *Homarus americanus*.<sup>17</sup> Weiss *et al.* have recently demonstrated by vibrational spectroscopy that ACC acts as a precursor phase for aragonite in mollusc larval shells.<sup>12</sup>

Crustaceans are excellent models to investigate biomineralisation. Many crustaceans have a rigid cuticle which contains an organic matrix and large amounts of CaCO<sub>3</sub> as the main mineral component. This cuticle cannot expand during growth of the animal. Hence, it is shed regularly during growth and replaced by a larger cuticle. During this moulting process calcium which is left within the old cuticle is lost and must be replaced to mineralise the new cuticle. In a marine environment calcium is readily available from seawater and most crustaceans can quickly replace lost calcium by taking up Ca<sup>2+</sup> from the

seawater across the gills.<sup>21</sup> Therefore, storage or recycling of calcium is of rather low significance for marine crustaceans. Terrestrial crustaceans, however, are under high environmental pressure to store and recycle calcium since they can replace lost calcium with food or freshwater only.<sup>22</sup>

About half of the 9000 known isopod species belong to the terrestrial isopods (*Oniscidea*), which among crustaceans developed the most elaborate adaptations to the terrestrial environment and became fully independent from aquatic habitats. Therefore, terrestrial isopods are regarded as the only “true-terrestrial” group of the crustacea. Most terrestrial isopods store CaCO<sub>3</sub> in large deposits within the ecdysial space between the cuticle secreting epithelium and the old cuticle of the first four sternites (Figs. 1A, 2A). The formation of these CaCO<sub>3</sub> reservoirs is accompanied by an interesting sequence of resorption and deposition of cuticular calcium (Figs. 1B, 1C), linked to the unique biphasic moult of isopods<sup>23</sup> which moult first the posterior (tailside) and then the anterior (frontside) half of the body. Before the moult of the posterior cuticle (pre-moult, Fig. 1B), calcium ions and probably also carbonate ions are resorbed from the posterior cuticle and stored within the first four sternites.<sup>24</sup> During the short period of less than one day between the moult of the posterior and anterior half of the body (intramoult, Fig. 1C) the sternal deposits are fully dissolved and the calcium of the deposits and part of the calcium within the anterior cuticle is used to mineralise the new posterior cuticle.

For *P. scaber* the structure and composition of the deposits were investigated previously by light microscopy, electron microscopy and X-ray microprobe analysis.<sup>19,20,25</sup> The sternal deposits consist of a homogeneous layer of glassy appearance facing the epithelium and an opaque layer adjacent to the old cuticle (Fig. 2B). Electron microscopy has shown that the opaque layer is composed of numerous spherules with diameters of up to 1.7 µm. This spherular layer can be subdivided into a proximal (towards the body center) spherular layer consisting of free spherules (Fig. 2C) and a distal (towards the body surface) spherular layer composed of smaller spherules, which often appear fused together (Fig. 2D). Both the homogeneous layer and the spherules consist of an X-ray amorphous (probably hydrated) CaCO<sub>3</sub> compound and contain an organic matrix.<sup>19</sup>

**Table 1** Ca K-edge EXAFS data of ACC deposits in *Porcellio scaber*, together with EXAFS data for the three water-free crystalline calcium carbonate polymorphs and for monohydrocalcite

Sample	$E_0/\text{eV}$	First shell: oxygen			Second shell			Third shell			Fourth shell: six Ca	
		$N$	$R/\text{\AA}$	$10^3\sigma^2/\text{\AA}^2$	$N$	$R/\text{\AA}$	$10^3\sigma^2/\text{\AA}^2$	$N$	$R/\text{\AA}$	$10^3\sigma^2/\text{\AA}^2$	$R/\text{\AA}$	$10^3\sigma^2/\text{\AA}^2$
<i>Porcellio scaber</i> , sternal deposit of ACC	+0.33	3.8 <sup>a</sup>	2.38 <sup>a</sup>	14	1.4 C <sup>a</sup>	3.00	7	0.4 C <sup>a</sup>	3.72	1	3.89	109
Aragonite reference	-1.04	9 <sup>b</sup>	2.47	33	3 C <sup>b</sup>	2.98	3	3 C <sup>b</sup>	3.26	10	3.94	28
Calcite reference	-0.29	6 <sup>b</sup>	2.33	9	6 C <sup>b</sup>	3.27	35	6 O <sup>b</sup>	3.65	16	4.05	9
Vaterite reference	+1.62	6 <sup>b</sup>	2.37	7	2 O, 2 C <sup>b</sup>	3.09	21	—	—	—	4.24	15
Monohydrocalcite reference <sup>15</sup>	+1.3..1.5	7.4 <sup>a</sup>	2.37	9	1.5 C <sup>a</sup>	3.03	7	3 C <sup>a</sup>	3.36	0	—	—

<sup>a</sup> Fit result. <sup>b</sup> Number fixed to crystallographic value.

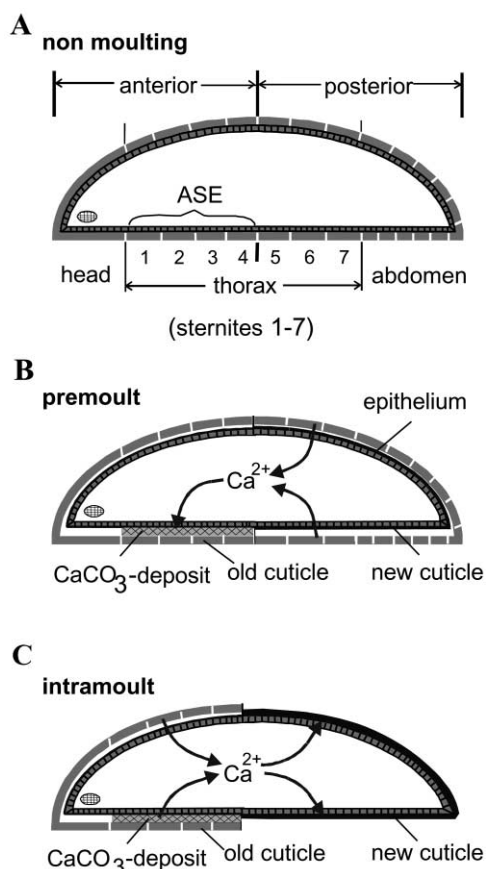


**Fig. 1** Schematic presentation of calcium fluxes in *Porcellio scaber*. (A) General morphology of *P. scaber*. (B) During premoult calcium from the posterior cuticle is resorbed into the hemolymph and transported across the anterior sternal epithelium (ASE) to sternal  $\text{CaCO}_3$  deposits. (C) After moulting of the posterior half of the body, calcium from the deposits and the anterior cuticle is resorbed and used to mineralise the new posterior cuticle. Arrows: direction of  $\text{Ca}^{2+}$  fluxes. Modified from ref. 35.

In order to further characterise the structure of the sternal  $\text{CaCO}_3$  deposits we applied high resolution X-ray diffractometry (XRD), X-ray absorption spectroscopy (Extended X-ray absorption fine structure; EXAFS) and reflection infrared microscopy (IR). The results are compared with literature EXAFS data obtained on X-ray amorphous calcium carbonate (ACC) by other authors. For comparison, the three crystalline anhydrous polymorphs of  $\text{CaCO}_3$  (calcite, aragonite and vaterite) were also studied by EXAFS.

## Results and discussion

Field-emission scanning electron micrographs of cleaved surfaces of the homogeneous layer and of spherules show that the spherical deposits consist of particles between 10 and 30 nm in

size (Figs. 2E, 2F). High-resolution high-intensity X-ray diffraction was performed on isolated sternal deposits (mineral phase only). Fig. 3 shows that there are no visible diffraction peaks at all, *i.e.* there are not even traces of crystalline phases present (detection limit about 0.5 to 1 wt%). If we assume Scherrer broadening of the diffraction peaks, we can estimate that the size of the coherently scattering domains must be smaller than  $\sim 100$  Å.

For further structural elucidation, X-ray absorption spectroscopy (EXAFS) at the calcium K-edge was employed. Fig. 4 shows the primary EXAFS oscillations, Fig. 5 shows the Fourier transform magnitude of this spectrum together with a fit to a suitable model. For comparison, the results for the crystalline phase vaterite are also shown. As the structure of this ACC phase is unknown, a suitable model derived from crystalline calcium carbonate was used. Table 1 contains the fit results, together with reference data. A comparison to the crystalline calcium carbonate phases is possible by analysing the first coordination sphere that always consists of oxygen. As EXAFS is very sensitive for coordination distances of the first shell (about  $\pm 0.02$  Å), these values are characteristic for the short-range order. For the three crystalline phases calcite, aragonite and vaterite, the Ca-6 Ca shell at about 4 Å is also important as the coordination number is always the same. The two other shells between 3 and 3.8 Å are less characteristic to distinguish between the different polymorphs as they differ considerably in the different calcium carbonate phases in distance and nature of neighbouring atom (C, O) (see Table 1). Another pseudopolymorph is monohydrocalcite  $\text{CaCO}_3 \cdot \text{H}_2\text{O}$  for which EXAFS fit data for the first shells are available.<sup>15</sup>

We can conclude from the fit results for the first shell that the calcium–oxygen distance in this ACC phase resembles either vaterite or monohydrocalcite. The coordination number  $N$  for Ca–O of 3.8 is associated with an estimated error of about 30%, but is closer to 6 (calcite, vaterite) or 7.4 (monohydrocalcite) than to 9 (aragonite). We do not make definite statements for the higher shells as they are all rather weak. The characteristic fourth shell (Ca-6 Ca) is especially weak in the sternal deposits as indicated by the high Debye–Waller factor (see also the Fourier transform magnitude in Fig. 5). These observations indicate a high degree of disorder in this ACC phase beyond the first coordination shell. We can conclude that the mineral has a well-defined short-range order in the first coordination shell with calcium coordinated by carbonate groups *via* the oxygen atoms. The coordination number is closer to 6 than to 9.

Table 2 shows the EXAFS data from the literature for all ACC phases investigated with this technique so far. It is evident that not all ACC phases are identical in structure. To cite from Sagi *et al.*:<sup>17</sup>

...the general term ‘amorphous calcium carbonate’ includes materials that are structurally different. These differences may account for the various mechanisms of their formation and stabilisation...

**Table 2** Results reported in the literature for EXAFS spectra of X-ray amorphous calcium carbonates found in biology, together with crystalline phases. The entries are sorted with ascending distance of the first coordination shell of oxygen. The second, third and fourth shells in the sternal deposits of *Porcellio scaber* are weak and of poor significance

Sample	Shell distance by EXAFS (Å)			
	First shell: Ca–O	Second shell: Ca–C or Ca–O	Third shell: Ca–C or Ca–O	Fourth shell: Ca–6 Ca
ACC in carapaces of <i>Homarus americanus</i> <sup>17</sup>	2.27	— <sup>a</sup>	3.47	3.79
ACC in plant cystoliths of <i>Ficus microcarpa</i> <sup>17</sup>	2.31	— <sup>a</sup>	3.48	3.79
Calcite (this work)	2.34	3.30	3.64	4.05
Calcite <sup>13</sup>	2.35	3.23	3.48	3.98
ACC in plant cystoliths of <i>Ficus retusa</i> <sup>13</sup>	2.36	3.22	3.39	4.06
Calcite <sup>15</sup>	2.37	3.21	3.52	4.11
Monohydrocalcite <sup>15</sup>	2.37	3.03	3.36	— <sup>a</sup>
Vaterite (this work)	2.37	3.09	— <sup>a</sup>	4.24
ACC in spicules of <i>Pyura Pachydermatina</i> <sup>15</sup>	2.37	3.03	3.36	— <sup>a</sup>
ACC in sternal deposits of <i>Porcellio scaber</i> (this work)	2.38	3.00	3.72	(3.89)
ACC in larval shells of <i>Biomphalaria glabrata</i> <sup>9,11</sup>	2.44	— <sup>a</sup>	— <sup>a</sup>	3.92
Aragonite (this work)	2.47	2.98	3.26	3.94

<sup>a</sup> Shell not included in fit.

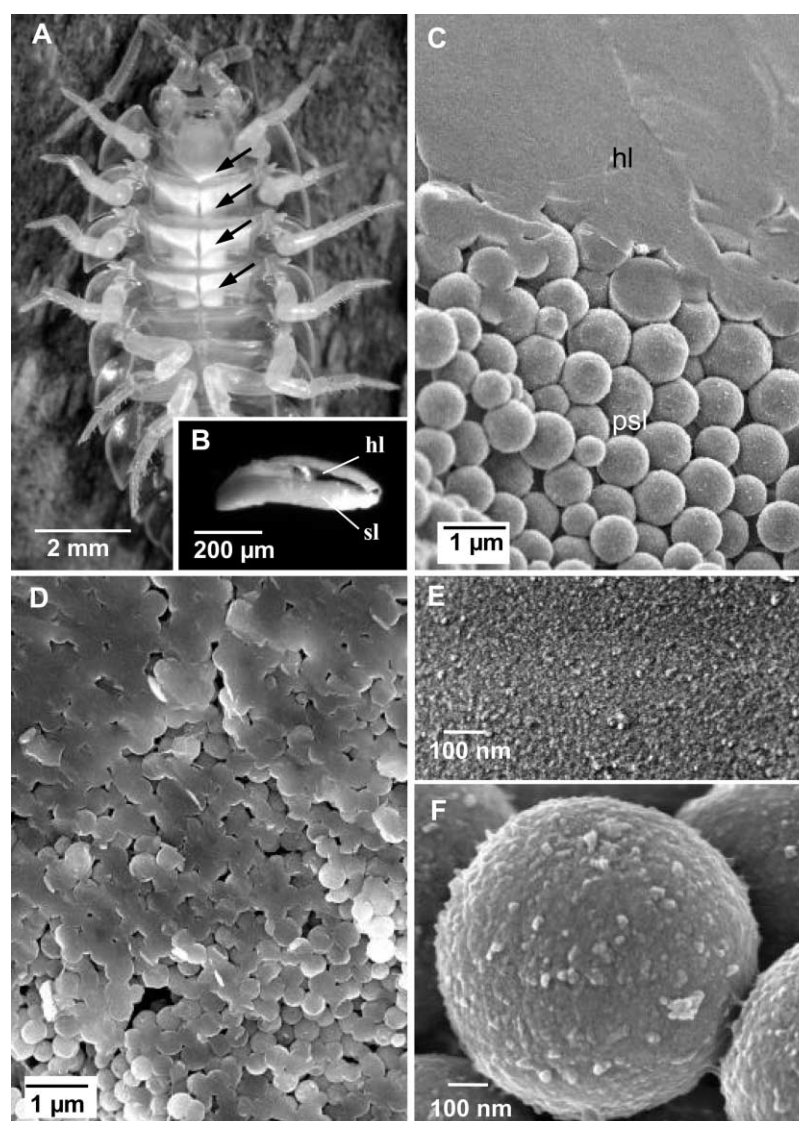


**Fig. 2** Structure of the sternal  $\text{CaCO}_3$  deposits of *Porcellio scaber* in late premoult. (A) Light micrograph of the ventral body surface showing the four sternal  $\text{CaCO}_3$  deposits (arrows). (B) Light micrograph of a  $\text{CaCO}_3$  deposit fractured in its central region showing the proximal homogeneous layer (hl) of glassy appearance and the distal spherular layer (sl). (C) Overview of the homogeneous layer and the proximal part of the spherular layer of  $\text{CaCO}_3$  (psl). (D) Overview of the distal spherular layer. (E) Surface structure of the homogeneous layer in high magnification. (F) Surface structure of a spherule.

In this particular case of the sternal deposits, the long-range order is particularly poor, *i.e.* we can assume that the thermodynamic stability is low, leading to a high solubility. As the

material is temporarily deposited for later remobilisation, this makes sense from the viewpoint of the organism.

Further information was derived from microscopic IR

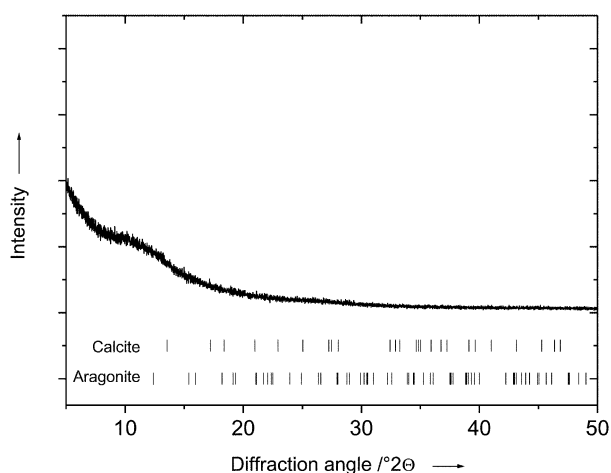


**Fig. 3** High-resolution X-ray powder diffractogram of sternal deposits of *Porcellio scaber* ( $\lambda = 0.90826 \text{ \AA}$ ). The diffraction peak positions that would be expected for calcite or aragonite are indicated for comparison. The material is fully X-ray amorphous.

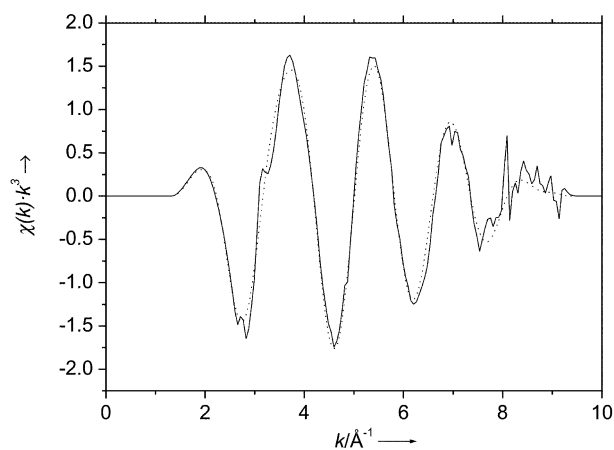


**Fig. 4** Primary Ca K-edge EXAFS data  $\chi(k)$  of sternal deposits of *Porcellio scaber*. Solid line: Experimental data. Dotted line: Fit data.

reflection spectra of the glassy natural surface (hl) and of the proximal spherular layer (psl) (see Fig. 2B). The data are shown in Fig. 6. These spectra reveal the presence of nanocrystalline calcium carbonate material with some degree of short-range order. In the range  $600\text{--}1500 \text{ cm}^{-1}$  calcium carbonate signals can be clearly distinguished from the excitations of organic components. The IR bands due to  $\text{CO}_3^{2-}$  vibrations in  $\text{CaCO}_3$  display excitations near  $1400$  and  $1480 \text{ cm}^{-1}$  ( $E_u$ ) and  $860 \text{ cm}^{-1}$  ( $A_{2u}$ ). The band near  $1400 \text{ cm}^{-1}$  shows strong intensity and might be induced by the small particle size of the crystallites. The bands at  $1400/1480 \text{ cm}^{-1}$  are due to the transverse optic (TO) component of the antisymmetrical stretching mode (for calcite: in the crystallographic  $ab$ -plane) whereas the band at  $860 \text{ cm}^{-1}$  corresponds to the longitudinal optic (LO) component of the out-of-plane mode (for E II c). Near  $710 \text{ cm}^{-1}$  the antisymmetrical bending mode  $E_u$  occurs in the  $ab$ -plane of the carbonate group. The excitations were assigned according to literature data.<sup>26–28</sup> Both spectra show similar bands, except one additional excitation which occurs in the homogeneous glassy surface (hl) near  $1630 \text{ cm}^{-1}$  (not related to calcium carbonate but probably to organic material).<sup>29</sup> Bands in the range of  $2000$  to  $3500 \text{ cm}^{-1}$  are likely to be caused by OH and water vibrations whereas the modes at higher energies are assumed to result from organic material. A comparison of the  $A_{2u}$  mode at  $860 \text{ cm}^{-1}$  with standard IR spectra of calcium carbonate<sup>29</sup> suggests that the structure resembles aragonite ( $860 \text{ cm}^{-1}$ ), but within the error limit calcitic ( $876 \text{ cm}^{-1}$ ) or vateritic ( $877 \text{ cm}^{-1}$ ) structures cannot be completely ruled out.

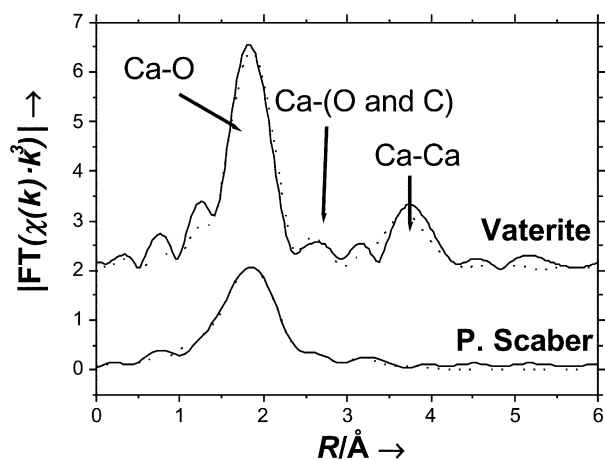


**Fig. 5** Ca K-edge EXAFS Fourier transform magnitude of well-crystalline vaterite (top) and of the X-ray amorphous sternal deposits of *Porcellio scaber* (bottom). The higher shells (especially Ca–Ca) show up to a much lesser extent in the ACC deposits compared to vaterite, indicating a high degree of disorder. Solid lines: Experimental data. Dotted lines: Fit data.

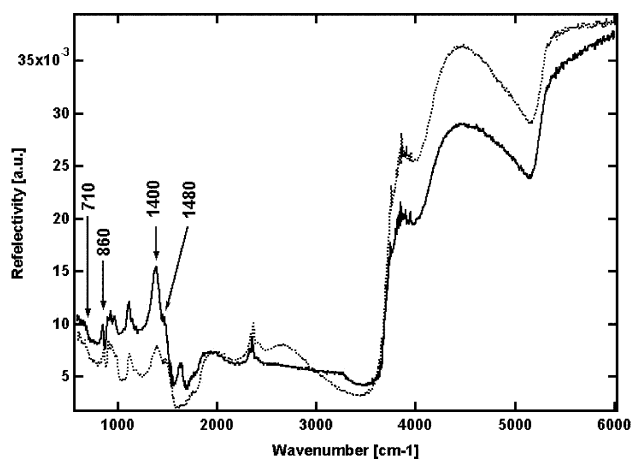


**Fig. 6** IR-reflection spectra of calcium carbonate surfaces displayed in Fig. 2B of *Porcellio scaber*. The solid line represents the spectrum of the homogeneous glassy layer (hl) and the dotted line that of the proximal spherular layer (psl). The indicated IR bands correspond to calcium carbonate (see text).

As the material leads only to diffuse X-ray diffraction but to excellent infrared light scattering signals we conclude that the particle size of the corresponding coherent lattice must be smaller than about  $100 \text{ \AA}$  (as estimated from Scherrer broadening of diffraction peaks) but larger than a few interatomic distances. Corresponding signals have been observed in the case of small clusters of ferroic materials<sup>30</sup> which were of the order of  $30 \text{ \AA}$ .

In conclusion, it could be shown that the sternal deposits are fully X-ray amorphous, but that they are not without structure. This corresponds well to results obtained for other biogenic ACC phases (Table 2). There is a defined first-shell coordination of oxygen around calcium, and the primary particle size is of the order of a few nanometers. The question how the material is prevented from crystallisation under ambient conditions and how it is precipitated must await further studies on the biological side of this system. However, it has been shown that specialised proteins are able to nucleate and stabilise amorphous calcium carbonate (which is almost impossible to prepare in the laboratory).<sup>8,14</sup> After all, a delicate interaction between biological compounds and the inorganic material is present in this kind of material.

## Experimental

Woodlice (*Porcellio scaber* Latr., 1804) were bred in plastic containers filled with soil and bark and fed on oak leaf litter and fresh potatoes. We identified animals in the premoult stage by their sternal deposits that can be seen as white spots at the ventral side (belly) of the living individuals. About 20 animals with well-developed sternal deposits were sacrificed and the cuticle and CaCO<sub>3</sub> deposits of the sternites 1–4 were gently removed, washed in bi-distilled water for about one second to remove any remaining body fluids (which have a high concentration of Na, Mg, K, Ca, and Cl).<sup>31</sup> In order to prevent (re-)crystallisation of ACC, the washing water was quickly removed by dipping the specimens in 100% methanol for about another second. Preliminary experiments showed that treatment with 100% methanol for one month had no apparent effect on the high-resolution X-ray diffraction patterns of the CaCO<sub>3</sub> deposits, *i.e.* no crystallisation occurred (data not shown). Then the specimens were air-dried and the CaCO<sub>3</sub> deposits were carefully removed from the cuticle using fine tweezers and collected to yield about 10 mg of material.

For field-emission scanning electron microscopy, sternites of animals in the late premoult stage were prepared as described above. CaCO<sub>3</sub> deposits were cleaved, mounted and rotary shadowed with platinum (2 nm) in a Balzers BAF 300 freeze-fracturing device and viewed with a Hitachi S-5200 field emission scanning electron microscope at acceleration voltages of 4 and 10 kV using a secondary electron detector.

EXAFS experiments were carried out at the Hamburger Synchrotronstrahlungslabor (HASYLAB) at Deutsches Elektronen-Synchrotron (DESY), Hamburg, at beamline E4. The DORIS III storage ring was operated at 4.5 GeV positron energy and currents of 70–150 mA. The incoming synchrotron beam was monochromated by a Si double-crystal. Experiments were performed at the Ca K-edge (*ca.* 4038 eV) in transmission mode at liquid nitrogen temperature. The slightly ground samples were fixed in a thin layer on adhesive tape. For quantitative data evaluation we used the programs SPLINE and XFIT.<sup>32</sup> Theoretical standards were computed with the program FEFF 6.01a.<sup>33</sup> All fits were carried out with  $k^3$ -weighted data in  $R$ -space. The amplitude reduction factor  $S_0^2$  was fixed to 0.60. For the reference compounds calcite, aragonite and vaterite, the coordination numbers were kept to the values derived from the crystal structure. For the ACC sample, the coordination numbers were allowed to vary. The error in this variable coordination number is about  $\pm 30\%$  as there is a strong mathematical correlation with the Debye–Waller factor  $\sigma^2$ . The typical error margin of EXAFS experiments for the first shell distance is about  $\pm 0.02$  Å.<sup>34</sup> These estimated errors are significantly higher for the second, third and fourth shells which are less well defined. The experimental data shown in Fig. 4 were treated with a window function but not Fourier-filtered.

High-resolution X-ray powder diffractometry was carried out in transmission geometry at room temperature (ground samples on Kapton foil) at beamline B2 at HASYLAB/DESY, Hamburg, Germany, at a wavelength of  $\lambda = 0.90826$  Å.

Unpolarised IR spectra between 600 and 6000 wavenumbers were recorded using a Bruker IFS 55 spectrometer equipped with a microscope, the beam diameter was about 100  $\mu\text{m}$  with 512 spectral scans per sample.

## Acknowledgements

The authors thank the Deutsche Forschungsgemeinschaft for support within the research program “Principles of Biomineralisation”. M. E. also thanks the Fonds der Chemischen Industrie for financial support. We thank C. Günther and G. Wolf, Freiberg/Sachsen, for providing the sample of phase-pure vaterite. Beamtime at the Hamburger Synchrotronstrahlungslaboratorium (HASYLAB at DESY) was generously provided.

## References

- 1 H. A. Lowenstam and S. Weiner, *On biomineralisation*, Oxford University Press, Oxford, 1989.
- 2 S. Mann, ed., *Biomimetic materials chemistry*, VCH, Weinheim, 1996.
- 3 S. Weiner and H. D. Wagner, *Annu. Rev. Mater. Sci.*, 1998, **28**, 271.
- 4 E. Baeuerlein, ed., *Biomineralisation*, VCH, Weinheim, 2000.
- 5 S. Mann, *Biomineralisation*, Oxford University Press, Oxford, 2001.
- 6 S. V. Dorozhkin and M. Epple, *Angew. Chem., Int. Ed.*, 2002, **41**, 3130.
- 7 L. Brecevic and A. E. Nielson, *J. Cryst. Growth*, 1989, **98**, 504.
- 8 E. Beniash, J. Aizenberg, L. Addadi and S. Weiner, *Proc. R. Soc. London B*, 1997, **264**, 461.
- 9 B. Hasse, H. Ehrenberg, J. C. Marxen, W. Becker and M. Epple, *Chem. Eur. J.*, 2000, **6**, 3679.
- 10 S. Raz, S. Weiner and L. Addadi, *Adv. Mater.*, 2000, **12**, 38.
- 11 J. C. Marxen, W. Becker, D. Finke, B. Hasse and M. Epple, *J. Mollusc. Stud.*, 2003, **69**, in press.
- 12 I. M. Weiss, N. Tuross, L. Addadi and S. Weiner, *J. Exp. Zool.*, 2002, **293**, 478.
- 13 M. G. Taylor, K. Simkiss, G. N. Greaves, M. Okazaki and S. Mann, *Proc. R. Soc. Lond. B*, 1993, **252**, 75.
- 14 J. Aizenberg, G. Lambert, L. Addadi and S. Weiner, *Adv. Mater.*, 1996, **8**, 222.
- 15 Y. Levi-Kalishman, S. Raz, S. Weiner, L. Addadi and I. Sagi, *J. Chem. Soc., Dalton Trans.*, 2000, 3977–3982.
- 16 J. Aizenberg, G. Lambert, S. Weiner and L. Addadi, *J. Am. Chem. Soc.*, 2002, **124**, 32.
- 17 Y. Levi-Kalishman, S. Raz, S. Weiner, L. Addadi and I. Sagi, *Adv. Funct. Mater.*, 2002, **12**, 43.
- 18 S. R. Wood and J. D. Russel, *Crustaceana*, 1987, **53**, 49.
- 19 A. Ziegler, *J. Struct. Biol.*, 1994, **112**, 110.
- 20 A. Ziegler and B. Miller, *Zoomorphology*, 1997, **117**, 181.
- 21 D. S. Neufeld and J. N. Cameron, *J. Exp. Biol.*, 1993, **184**, 1.
- 22 P. Greenaway, *Biol. Rev.*, 1985, **60**, 425.
- 23 B. Messner, *Crustaceana*, 1965, **9**, 285.
- 24 C. G. H. Steel, *Can. J. Zool.*, 1993, **71**, 4.
- 25 A. Ziegler, *Cell Calcium*, 2002, **31**, 307.
- 26 V. C. Farmer, *The Infrared Spectra of Minerals*, Mineralogical Society, London, 1974.
- 27 K. Nakamoto, *Infrared spectra of inorganic and coordination compounds*, Wiley, Weinheim, 1978.
- 28 J. C. Decius and R. M. Hexter, *Molecular Vibrations in Crystals*, McGraw-Hill, New York, 1987.
- 29 G. Falini, S. Albeck, S. Weiner and L. Addadi, *Science*, 1996, **271**, 67.
- 30 U. Bismayer, *Rev. Mineral. Geochem.*, 2000, **39**, 265.
- 31 A. Ziegler and F. H. E. Scholz, *J. Comp. Physiol., B*, 1997, **167**, 536.
- 32 P. J. Ellis and H. C. Freeman, *J. Synchrotron Rad.*, 1995, **2**, 190.
- 33 S. I. Zabinsky, J. J. Rehr, A. Ankudinov, R. C. Albers and M. J. Eller, *Phys. Rev. B*, 1995, **52**, 2995.
- 34 H. Bertagnolli and T. S. Ertel, *Angew. Chem., Int. Ed. Engl.*, 1994, **33**, 45.
- 35 A. Ziegler, D. Weihrauch, D. W. Towle and M. Hagedorn, *Cell Calcium*, 2002, **32**, 131.